Simulation and Analysis of Antibody Aggregation on Cell Surfaces Using Motion Planning and Graph Analysis

Kasra Manavi
Dept. of Computer Science
University of New Mexico
Albuquerque, New Mexico, 87131
kazaz@cs.unm.edu

Bridget S. Wilson
Dept. of Pathology and Cancer Research and Treatment Center
University of New Mexico
Albuquerque, NM 87131
bwilson@salud.unm.edu

Lydia Tapia
Dept. of Computer Science
University of New Mexico
Albuquerque, New Mexico, 87131
tapia@cs.unm.edu

ABSTRACT

IgE antibodies bound to cell-surface receptors, FcεRI, crosslink through the binding of antigens on the cell surface. This formation of aggregates is what simulates mast cells and basophils in order to initiate an allergic response. Experimental studies have shown that the spatial organization of aggregated IgE-FcεRI complexes affect transmembrane signaling that initiate these responses. About 1,500 Americans die each year from anaphylatic shock caused by these aggregations.

The methods we present in this paper address modeling and analyzing this critical molecular data. First, we developed 3D models of a trivalent antigen and IgE-FcεRI complex binding using relaxed constraints. Simplified models were generated from all-atom structures to reduce the complexity of the geometry and are simulated on a plane to capture movement of antibodies on the cell surface. This reduces the computational complexity of the simulation to a rigid body problem, often addressed in motion planning. Motions and resulting aggregations are extracted from Monte Carlo simulations with kinetic rates derived from experiments. In order to analyze the resulting structures, we introduce techniques to map 3D molecular binding to a graph structure. This facilitates analysis of aggregate structures because simple graph metrics, such as connected components and subgraph isomorphism, can be used to quickly quantify and analyze aggregate structure.

Categories and Subject Descriptors

I.2.9 [**Robotics**]: Workcell Organization and Planning; I.6.8 [**Simulation and Modeling**]: Monte Carlo; G.2.2 [**Discrete Mathematics**]: Graph Theory; J.3 [**Computer Applications**]: Biology and Genetics

1. INTRODUCTION

Each year in the United States, about 1,500 people die from anaphylactic shock [22]. This is caused by a tyrosine kinase cascade initiated by antigen-mediated crosslinking of IgE, bound to its receptor FcεRI. This crosslinking process stimulates both mast cells and basophils to then release histamine and other mediators of allergic reactions [18]. Previous studies suggest the spatial organization of clustered IgE-FcεRI complexes significantly affects the transmembrane signaling which initiates these responses [28, 27, 26, 6]. Trivalent ligands have been shown to provide the minimal structural requirements for FcεRI activation leading to degranulation in a rat mast cell model system, the 2H3 line of rat basophilic leukemia (RBL-2H3) cells [20, 13]. In this work we introduce models for simulating and analyzing cell-surface receptor aggregation.

We apply ideas from both robotic motion planning and graph theory. Robotic motion planning has been applied to many complex planning problems including modeling the motions of many robotic agents [4]. Motion planning has also been used to study protein folding [1, 25, 24], RNA folding [23], and ligand binding [21, 3]. Graph theory has been applied to many biological problems including antibody-antigen reactivity [12] and antibody response quality [8].

Our method uses 3D models of a trivalent antigen and IgE-FcεRI complex binding using relaxed constraints. The method begins by producing geometrically simplified versions of the molecules to facilitate animation and simulation. These simplified models were generated from all-atom structures. This significantly reduces the complexity of the motions by reducing the simulation to a rigid body problem, often addressed in motion planning. We simulate the molecular interaction using a Monte Carlo approach with relaxed constraints and analyze the resulting antigen/IgE aggregations. We vary the ratio of ligand to receptor and include association and dissociation rates. During analysis we show the formation of aggregate structures on a set of varied receptor to ligand ratios using graph analysis techniques.

This paper's contributions are the following:

- The introduction of a model for the IgE-FcεRI receptor and trivalent ligand interaction using experimental structural data of the molecules.
- Methodologies for simulating the motion and binding of the molecules that incorporate biologically derived parameters.
- A novel way to classify and compare receptor aggregations using graph analysis.

We are able to show that this geometric model is well suited to study antigen/IgE interactions and is easily extendable. The use of 3D geometry allows us to include more biologically relevant structural data, increasing the accuracy of our simulation over prior simulations. Using 3D geometry also increases flexibility in future experiments, allowing for the use of a variety of molecular structures.

2. RELATED WORK

2.1 Motion Planning

One of the major problems in robotics is that of finding a valid, collision-free path for a robot through a given environment. Motion planning [17] has been extensively studied and has applications in a variety of domains, including the study of molecular motions [21, 1].

In motion planning, a robot is a moveable object whose position and orientation can be defined by d parameters, or degrees of freedom (DOFs). These parameters define the robots placement, or configuration, in an environment. These d parameters can be used to describe the robot as a point in a d-dimensional space. This space is referred to as configuration space, or C_{space} and includes all possible configurations, valid and invalid [11]. All valid, or feasible, configurations are considered to be in the subset C_{free} and all invalid, or infeasible, configurations are in C_{obst}. The motion planning problem has now become a problem of finding a valid series of configurations in C_{free} between start and goal configurations. In our work here, we do not specify a goal configuration. Rather, we explore C_{free} until a convergence criterion is met.

Molecular motions have been simulated using a variety of methods. Monte Carlo simulations are a way explore molecular motions while defining clear time intervals for simulation [5, 10]. Some recent simulation approaches stem from the idea of motion planning. In this work, the motions of protein folding [1, 25, 24], RNA folding [23], and ligand binding [21, 3] have been simulated.

2.2 IgE Aggregation Experiments

Experimental studies of IgE aggregation require nanoscale resolution of membrane sheets. Recent experimental advances using Transmission Electron Microscopy (TEM) have enabled researchers to view the motions of immunogold-labeled FcεRI [26]. This technology produces images in which the nanogold particles appear as clustered black dots during aggregation. Metrics, e.g., particle speed, can be measured from image sequences [2]. However, these experimental studies are limited because there is no information provided about binding patterns. Therefore, it is difficult, if not impossible, to distinguish an aggregate from a group of molecules that are simply proximal.

2.3 IgE Aggregation Models & Simulations

A series of planar models have been developed which model the ligand-receptor interaction [7, 31, 15]. All these models assume trivalent ligands binding with a bivalent cell surface receptor in a well-mixed system. It is also assumed that the binding sites on both ligand and receptor are identical, and a single ligand cannot bind to both sites of a receptor. The first model, the Goldstein-Perelson model is based on thermodynamic equilibrium and takes into account two interactions [7]. The first is between a free ligand and a free receptor. The second is the cross linking of of two receptors by a ligand. This model accounts for some aggregate structures. However, it fails to adequately account for cyclic aggregates. A newer model called the TLBR model was developed as a kinetic version of the Goldstein-Perelson model [31]. This model takes into account cyclic aggregates that form dimers and hexagonal aggregates. These models were put into a simulation which took into account steric constraints of the interactions [15].

Simulating molecular interactions and aggregations using multiscale approaches (using a combination of low and high resolution data) is becoming a popular trend. A prime example is seen in work converting three dimensional affinities to 2 dimensional of membrane bound molecules [29]. This method uses the idea of a multiscale approach, using molecular dynamics to study the interdomain flexibility, Monte Carlo simulations to study multidomain motion and lattice simulations to study clustering.

3. METHODS

The methods used and developed include: construction of molecular models, simulating motions and aggregations, encoding the aggregations as graph structures, and analysis of the aggregations.

3.1 Model Construction

We use 3D models of the ligand and receptor molecules in our simulation. The initial all-atom molecular structure models used in our simulations were generated in [13]. These models were created using the motif binding geometries, homology modeling and molecular dynamics. The receptor complex model was constructed using available molecular PDB structures (PDBs: 1OAU, 2VWE, 1O0V, 1F6A). The IgE structure is 1,532 amino acids (11,850 atoms) and is modeled bound to FcεRI. The ligand is a fibritin trimer has a known structure (PDB: 1RFO), and is 371 amino acids (5176 atoms) large. In order to bind with IgE, the N-terminus of each fibritin is extended with a flexible DNP linker, about 1 nm in length.

Using complete structures for simulation would have been computationally expensive, so the isosurface of these molecules was calculated to form a high resolution 3D structure of the occupied volume of the molecule. The isosurface was calculated using the Chimera [16] molecular viewer/modeler. The high-resolution object files contain a large amount of detail which effects performance, e.g., collision checking, with hundreds of moving molecules.

The structure was then reduced to a smaller number of polygons to decrease the complexity of the surface. The high-resolution structure went through a polygon reduction algorithm using the Maya modeling software package. These simplified structures are used to model the molecule in simulation. The model construction process is shown in Figure 1.

3.2 Simulation Algorithm

Our algorithm models the molecular interactions using a simple Monte Carlo type simulation. We formulated a graph-based structure to define the molecular interactions. In these graphs, there are two classes of molecules, receptors and ligands, which are represented as vertices in the graph with different labels. Receptors have two binding sites and ligands have three. If a receptor binds with a ligand, it forms an edge in the graph to represent the linking. This structure allows us to encode the molecular structure in a simple representation to maintain during simulation and to further analyze aggregates and their structures.

Simulations are initialized with randomly placed receptors and ligands in a bounding volume in a collision-free state. Since nothing is bound in the initial state, the graph, G, begins with with vertices and no edges. The molecules are allowed to move on the XY plane and rotate about the Z

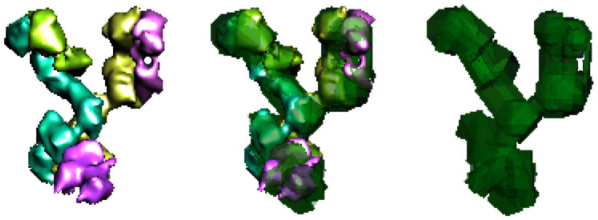

Figure 1: Models were polygonal reductions of the iso-surface of the all-atom molecular structure. This process occurred in three steps: A.) the iso-surface of the original model, B.) the reduced polygon model overlaying the iso-surface, and C.) the reduced polygon model.

axis, defining 3 DOFs per molecule. The complexity of the simulation (total number of DOFs) depends primarily on the number of molecules simulated. For example, 20 molecules requires exploration of a 60 DOF C_{space}.

Algorithm 3.1 Simulation Algorithm

Input. Receptors R, ligands L and graph G.
Output. A set S of the resulting aggregates

```
Initialize(R,L,G)
for timestep = 0:MAX_TIME do
  for each molecule m ∈ R ∪ L do
    m.DetermineMotion(G)
    moleculeList old = m.KnownBoundSites()
    moleculeList new = m.PotentialBindingSites()
    for each t ∈ old do
      S.TryRemoveLink(G,m,t,D_RATE)
    end for
    for each t ∈ new do
      S.TryAddLink(G,m,t,A_RATE)
    end for
  end for
  if G.StabilityReached() then
    break()
  else
    G.StoreConnectionCount()
  end if
end for
set S = G.DetermineAggregates()
return S
```

Algorithm 3.1 outlines method used to move and bind the ligands and receptors. First, the simulation is initialized as defined above. At each time interval, a Monte Carlo step is taken and all positions of the molecules in the simulation are updated. This step is determined using random sampling, a technique often used to solve high-dimensional motion planning [9] problems. However, in this case the biological constraints of the system are considered, e.g., molecule speeds. Also, association and dissociation rates are included. This means that at each time step every pair of molecules that are within binding distance will bind with a probability defined by the association rate. Alternatively, each bound pair of molecules is probabilistically evaluated for bond breakage according to the dissociation rate. In terms of graph updates, association and dissociation relate to the creation and removal of edges.

As the molecules move in the bounding volume, ligands and receptors begin to bind and form aggregates. As the aggregates increase in size, the collection of molecules as a whole slows down and begins to move at a reduced speed. Simulations are run until a stopping criteria is met, e.g., stable graph formation. Figures 2 and 3 show small and large scale examples of our experiments.

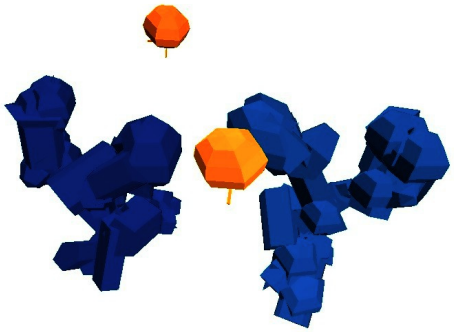

Figure 2: Small simulation with 2 receptors and 2 ligands. The 2 receptors (*blue*) are bound by a ligand (*yellow*), and there is a second free ligand.

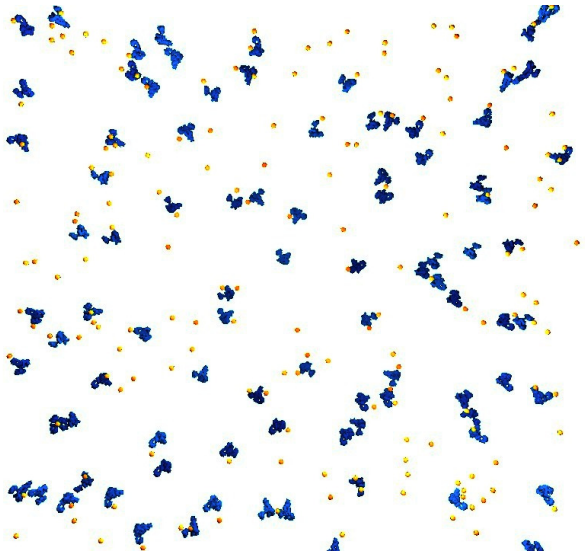

Figure 3: Large simulation with 90 receptors (*blue*)and 180 ligands (*yellow*). The state is near the beginning of the experiment, showing a well mixed system with some early binding.

3.3 Aggregate Model and Analysis

Each simulation provides a graph, G, representing the structure of aggregates and singletons produced. These graphs

can be analyzed using standard graph metric tools. For example, the number of edges in G should stabilize when the simulation reaches equilibrium. Also, the number of connected components in G measures the number of aggregates and singletons in the simulation.

Each aggregate is represented by a connected component, g, in G. Each g can be individually analyzed in order to quantify important characteristics. In this paper, we highlight two graph-based analysis that we can run on a connected component: aggregate classification and common aggregate structure. Classification is performed using a depth first search traversal, and commonly formed aggregate structure is performed through subgraph isomorphism.

3.3.1 Aggregate Classification

In order to characterize the aggregate structure, we used a graph traversal algorithm. Sample aggregates and their corresponding graph structures are shown in Figure 4. The characteristics of the aggregate structures allow us to define four major classifications:

- Singleton (1 receptor with at least 1 ligand bound)
- Linear Chain (2 or more receptors forming a chain)
- Cyclic n-mer (2 or more receptors forming a cycle)
- Complex Aggregate (3 or more receptors forming a combination of single bound receptors, linear chains and cyclic n-mers)

Examples each classification are in Figure 4. If an aggregate graph has two vertices, it must be a Singleton. If an aggregate graph has three vertices, two of which are ligands, it also will be labeled a Singleton. On the other hand, a graph with three vertices, where only one is a ligand, is a Linear Chain. Aggregate graphs of four vertices or larger are distinguished as Linear Chains, Cyclic n-mers, and Complex Aggregates. If these larger aggregate graphs are traversed and no repeated vertices are seen, it is labeled a Linear Chain. However, if a single cycle exists in the graph, then the structure is labeled a Cyclic n-mer where n refers to the number of receptors. The final structure, Complex Aggregate, is identified during aggregate graph traversal through the identification of multiple repeated molecules or extra molecules beyond those in a Cyclic n-mer. This means Complex Aggregates can be any combination of Linear Chains and Cyclic n-mers.

These classifications are based on experimental studies of IgE aggregation. The labeling of FcεRI with nanogold particles produces 2D plots of dark spots. Regular structures such as Linear Chains and Cyclic n-mers can be easier to identify and interpret about possible binding patterns. However, the remaining classifications can be difficult, if not impossible, to distinguish.

Classification is performed by traversing the aggregate graph using depth-first search. This produces a search tree where cycles and dead ends can be identified. Each of these is a feature that can be used to identify the four aggregate classifications. For example, Linear Chains have no cycles but do have dead ends. On the other hand, Cyclic n-mers have only cycles but no dead ends. Complex Aggregates consist of combinations of cycles and dead ends.

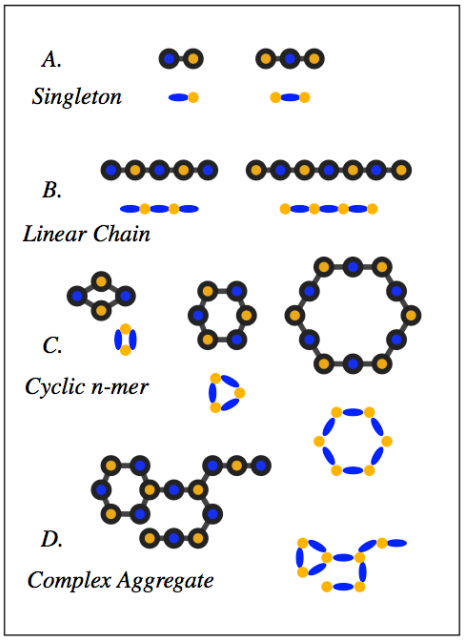

Figure 4: Aggregates can be represented as graphs that capture the binding of the receptors and ligands. The blue and yellow diagrams demonstrate sample receptor *(blue)* and ligand *(yellow)* binding patterns. The corresponding graph structures are shown above (a-c) and left (d). Graph nodes are labeled as ligand *(yellow with black outline)* and receptor *(blue with black outline)*. The aggregates are classified into 4 categories: *a.)* Singletons are just single receptors bound to a ligand or two, *b.)* Linear Chains are two or more receptors forming a sequential chain, *c.)* Cyclic n-mers are where two or more receptors form a cycle, and *d.)* Complex Aggregates are made up of combinations of linear chains and cyclic n-mers, in this case a cyclic trimer and two linear chains.

3.3.2 Common Aggregate Substructure

The ability to identify common aggregate substructure could provide insight into likely and common aggregate formations. In this paper, we use subgraph isomorphism in order to identify the largest and most frequently occurring aggregate formations. McGregor's common subgraph algorithm [14] can extract these substructures from the aggregate graphs produced by the simulation. After subgraphs are extracted, they also can be classified using the methods described above in Section 3.3.1.

4. RESULTS

For our experiment we keep the number of receptors consistent and vary the number of ligands. We used 90 receptors in our experiment and limited our ligand counts to 30, 45, 60, 90, 135, and 180. These combinations were chosen to match experimental analysis which keep consistent receptor concentration and vary ligand concentration. The bounding volume used was 400nm by 400nm and is fixed over the course of all experiments. The time interval used

was 13.2ms and is fixed for all simulations. Biologically derived parameters were used whenever possible. For example, the association and dissociation rates are 1.0 and 0.025, respectively. These values are based on experimental studies of IgE binding [30]. Recent experimental evidence suggests that unbound molecules move at faster rates than bound molecules [2]. In order to account for this, the base speed for molecules is s, $0.09\mu m^2/s$. As molecules aggregate, the speed of the aggregate i is adjusted to $s/|v_i|$ where v_i is the number of molecules in the aggregate. This adjusts the speed of the aggregate relative to its size.

Simulations were created using PMPL, a motion planning library developed at Texas A&M University and graph analysis was performed using elements of Boost Graph Library [19]. Experiments were run in a Linux environment on a single processor of an Intel i7 quad-core with 8G of RAM. Multiple (10) runs were done for each experiment.

4.1 Equilibrium of Aggregate Formation

Each aggregate analysis metric could be used during any point during simulation. However, the aggregates should be the most complex after the simulation is allowed to run to an equilibrium state. In these results, we quantified the stability of the graph G in terms of the number of edges. This is due to the fact that the addition and removal of edges indicates a change in aggregate structure.

The average number of edges in G is shown in Figure 5. Each run was for 36,000 timesteps the equivalent of 8 minutes real time. As can be seen in Figure 5, the number of edges quickly grew in all ratios of receptors to ligands. Near the two minute mark, all the curves begin to level off with much smaller growth in the number of edges. This means that the aggregates were mostly formed at two minutes but continue to change slowly as the simulation is run. This result is consistent with observations in changes of FcεRI mobility, which are associated with changes in aggregate size. Abrupt slowing of IgE-receptor aggregates can be observed within 20 secs of polyvalent ligand addition and are typically complete within 60-90 secs [2].

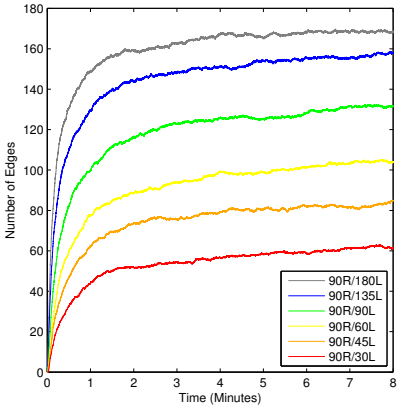

Figure 5: The number of edges was recorded each time step and used to estimate when the experiment reached a stable state. The x-axis is time in minutes and the y-axis is the number of connections

4.2 Aggregate Size

The electron microscopy approach has shown that large FcεRI "signaling patches" form within 1-2 minutes of addition of polyvalent antigen. One limitation of this technique is that, whicle these patches may contain tens to hundreds of FcεRI in complex with IgE and antigen, it is not possible to estimate the range of aggregate sizes within these signaling patches. In this section, we demonstrate the power of the graphing approach to estimate aggregate size.

Results are shown in Figure 6, where aggregate size was measured for every subgraph in G of three vertices or more. Aggregate size can be measured for every subgraph in G. The number of vertices will distinguish the size of the subgraph. However, since experimental studies are only able to distinguish receptor position, we measure aggregate size as the subset of vertices labeled as receptor. After the simulations were run, aggregate sizes were collected and averaged.

In Figure 6 there are clearly aggregate size differences depending on the ratio of ligand to receptor. With a low ratio, there are fewer ligands to receptors, so the receptors are unable to easily find an unbound ligand. However, since there is a low abundance of ligand, the aggregates do not get very large. Looking at the lowest ratio experiment, these aggregates had up to seven receptors (far left bar in Figure 6). With a high ratio, we see a saturation of ligands and a lack of receptors, leading to aggregates staying small. This is because the binding sites of the receptors are quickly filled with unbound individual ligands keeping aggregate size small, resulting in aggregates of at most size six (far right bar in Figure 6). The ratios which lie in the middle, show different characteristics than at the ratio extremes. As the number of ligands increase, the largest aggregate size increases till ligand saturation over takes the trend starts to decrease largest aggregate sizes. This can been seen in the bell shape curve in number of occurrences generated by the different experiments at individual receptor counts. We see larger aggregates, up to ten receptors, for runs with less disparate receptor to ligand ratios in Figure 6. However, these large aggregates are very uncommon in occurring in only a few of the runs for each ratio.

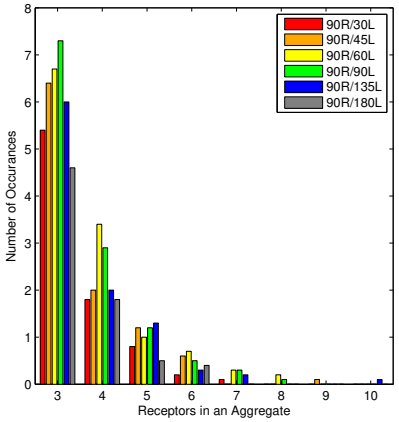

Figure 6: Histograms of aggregate size (as defined by number of receptors). Aggregate sizes were collected at the end of runs and averaged.

4.3 Aggregate Population Kinetics

Population kinetics defines the population of a class of

objects over time. In our case we define aggregate structure by the four classes defined in Figure 4. Given these four classes and an unbound receptor class, we can measure how the population of each class changes over the course of the simulation. In Figure 7 the class of every receptor is plotted against time for the full 8 minutes of simulated aggregation. Values are averaged over all ten runs.

The kinetics in all six plots shows more gradual change in class after 2 minutes of simulation. This relates to Figure 5 where the number of edges begins to converge after 2 minutes. Therefore, Figure 7 confirms that after about 2 minutes, the majority of aggregates are fully formed.

The first notable trait in Figure 7 is that the percentage of unbound (free) receptors decreases quickly in all six ratios. When there is a low ratio of ligand to receptor as in Figure 7(a), there are always some remaining free receptors. As the ligand to receptor ratio increases, the number of free receptors go down since there are more ligands to bind to the free receptors. We also see that at 20 secs, the percentage of free receptors in the lowest ratio is 70%, where in the highest ratio it is 10%. This matches results which shows that ligand concentration is related to the the speed of immobility (formation of aggregates) [2].

Recall that singleton refers to a single receptor bound to either one or two ligands. In the run where there are few ligands and many receptors (Figure 7(a)), we see a low percentage of singletons (magenta line), but we see this percentage increase as the ratio increases. This is due to the fact that unbound receptors have an easier time finding one or two unbound ligands in these high ratio cases.

Another fact that is evident from the plots in Figure 7 is that Cyclic n-mers are not very common in any case. This is due to the fact that the structure is very constrained. It requires that ligands and receptors to bind at angles that are optimized in order to form cycles. Another requirement is that nothing else can bind beyond those receptors needed for the cycle. This is unlikely given the three (one free) binding sites available in our ligand structure. Recall that if other structures extend off the Cyclic n-mer, it will be classified as a Complex Aggregate.

4.4 Aggregate Substructure Analysis

Common aggregate substructure can indicate those structures that are the most common (and possibly required) for the formation of larger aggregates. In this study, we took the two largest aggregates from each of the ten runs of the six ratios. Then, we performed McGregor's common subgraph between all pairs of a ratio's aggregates. In order to describe the resulting substructure, classification was run on the common subgraphs.

Two resulting common subgraphs are shown in Figure 8. Even though the two original aggregates had two different classes (Complex Aggregate and Linear Chain for a and b, respectively), their common subgraph was a Linear Chain of three receptors and three ligands. The vertices that are part of the subgraph are circled and labeled with numbers for easier comparison. The vertices are in positions that relate to their center of mass of the molecules. However, the vertices are not scaled for the size of the molecule.

Table 4.4 outlines the classifications of the subgraphs identified from pairwise comparison. Recall, that the pairwise comparison takes the two largest aggregates from each of the ten simulations for a ratio and finds their common subgraph.

	low ⟶ ligand ratio ⟶ high					
Classification	30L	45L	60L	90L	135L	180L
Linear Chain	48%	36%	45%	90%	86%	89%
Cyclic n-mer	0%	0%	0%	0%	0%	0%
Complex Agg	52%	64%	55%	10%	14%	11%

Table 1: Classification of the most common subgraphs extracted from pairwise aggregate comparison. 90 receptors were used for all runs.

In these results, there appears to be a relationship between common subgraph classification and the ratio of receptors to ligands. With few ligands (lower three experimental ratios), there was an even ratio of linear chains and complex aggregates found as the subgraph isomorphism. However, there is increase in Linear Chains when the saturation of ligands increases. In the three highest ratio experiments, we see a much higher ratio of linear chains versus complex aggregates as the common substructure. We note that in the kinetic results that at the highest two ligand to receptor ratios, complex aggregates overtake linear chains in classification. Linear chain geometry appears to be better suited for generating large aggregates in high ratio experiments.

5. CONCLUSIONS

In this paper, we presented methodologies for simulating and analyzing aggregate formation from the cross-linking of an antibody to a trivalent antigen. By developing simplified models based on experimentally derived data, we are able to study aggregate formation under biologically-relevant conditions. This is particularly helpful since experimental techniques report proximity of clustered receptors but fail to provide a measurement of aggregate sizes within a complex topography. Our 3D simulations have provided unique insight into the aggregation process by reporting both realistic timescales and by classifying the most common geometry associated with receptor aggregates.

The methods provided are based on techniques from both motion planning and graph analysis. That makes them simple to implement and easily adaptable to changes in the problem structure. For example, studying a different receptor structure would entail a change in model. Also, graph analysis is general, and can be applied to any resulting aggregate graph structure.

6. ACKNOWLEDGMENTS

This work supported in part by the National Institutes of Health (NIH) Grant P50GM085273 supporting the New Mexico Spatiotemporal Modeling Center and NIH Grant P20RR018754 supporting the Center for Evolutionary and Theoretical Immunology. Special thanks to Chang-Shung Tung from Los Alamos National Laboratories for providing the structures used, and the Adaptive Motion Planning Research Group members Andrea Howells and Nick Malone for help with the modeling and algorithm format.

7. REFERENCES

[1] N. M. Amato, K. A. Dill, and G. Song. Using motion planning to map protein folding landscapes and analyze folding kinetics of known native structures. *J. Comput. Biol.*, 10(3-4):239–255, 2003.

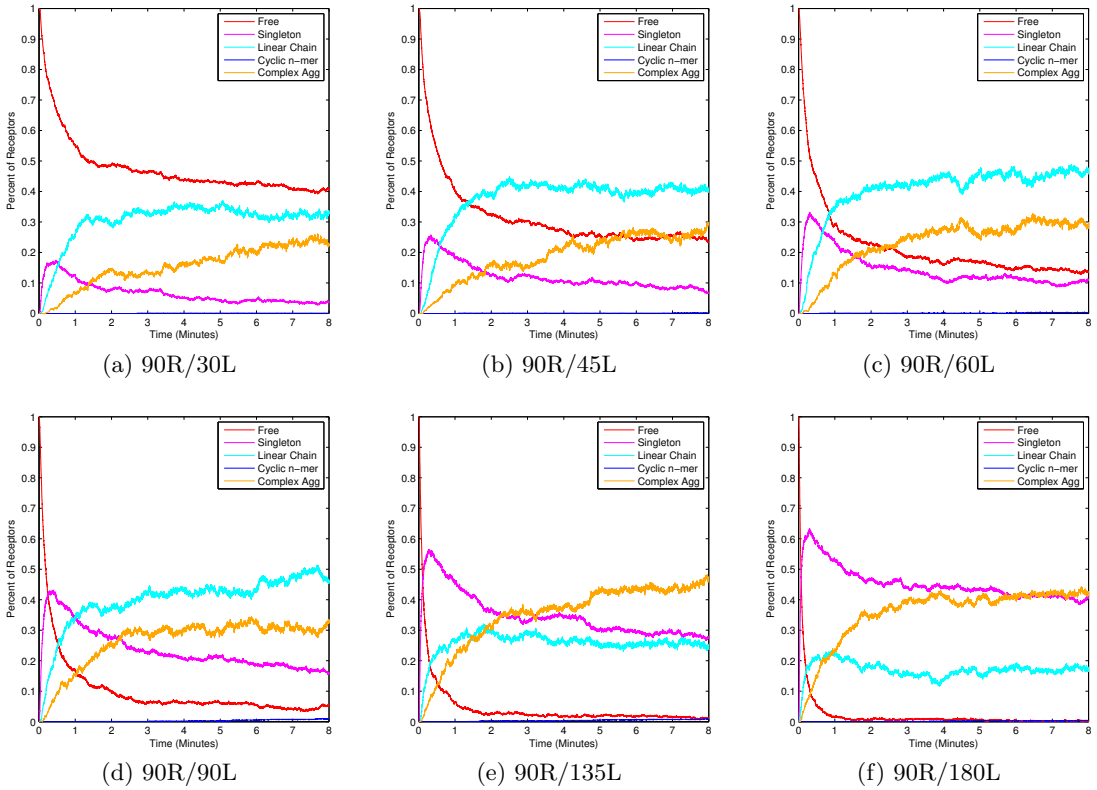

(a) 90R/30L (b) 90R/45L (c) 90R/60L

(d) 90R/90L (e) 90R/135L (f) 90R/180L

Figure 7: Population kinetics for studied ratios of ligand to receptor.

[2] N. L. Andrews, J. R. Pfeiffer, A. M. Martinez, D. M. Haaland, R. W. Davis, T. Kawakami, J. M. Oliver, B. S. Wilson, and D. S. Lidke. Small, mobile FcεRI receptor aggregates are signaling competent. *Immunity*, 31(3):469–479, 2009.

[3] O. B. Bayazit, G. Song, and N. M. Amato. Ligand binding with OBPRM and haptic user input: Enhancing automatic motion planning with virtual touch. In *Proc. IEEE Int. Conf. Robot. Autom. (ICRA)*, pages 954–959, 2001.

[4] K. E. Bekris, K. Tsianos, and L. E. Kavraki. A decentralized planner that guarantees the safety of communicating vehicles with complex dynamics that replan online. In *Proc. IEEE International Conference on Intelligent Robots Systems (IROS)*, 2007.

[5] D. Covell. Folding protein α-carbon chains into compact forms by Monte Carlo methods. *Proteins: Struct. Funct. Genet.*, 14(4):409–420, 1992.

[6] C. Fewtrell and H. Metzger. Larger olilgomers of IgE are more effective than dimers in stimulating rat basophilic leukemia cells. *J. Immunol.*, 125:701–710, 1980.

[7] B. Goldstein and A. Perelson. Equilibrium theory for the clustering of bivalent cell surface receptors by trivalent ligands. Application to histamine release from basophils. *Biophysical Journal*, 45(6):1109–1123, 1984.

[8] W. A. Howard, K. L. Gibson, and D. K. Dunn-Walters. Antibody quality in old age. *Rejuvenation Research*, 9(1):117–125, 2006.

[9] L. E. Kavraki, P. Švestka, J. C. Latombe, and M. H. Overmars. Probabilistic roadmaps for path planning in high-dimensional configuration spaces. *IEEE Trans. Robot. Automat.*, 12(4):566–580, August 1996.

[10] A. Kolinski and J. Skolnick. Monte Carlo simulations of protein folding. *Proteins Struct. Funct. Genet.*, 18(3):338–352, 1994.

[11] T. Lozano-Pérez and M. A. Wesley. An algorithm for planning collision-free paths among polyhedral obstacles. *Communications of the ACM*, 22(10):560–570, October 1979.

[12] A. Madi, D. Y. Kenett, S. Bransburg-Zabary, Y. Merbl, F. J. Quintana, A. I. Tauber, I. R. Cohen, and E. Ben-Jacob. Network theory analysis of antibody-antigen reactivity data: the immune trees at birth and adulthood. *PLOS One*, 6:1–11, March 2001.

[13] A. Mahajan, D. Barua, P. Cutler, D. S. Lidke, G. Zwartz, F. Espinoza, C.-S. Tung, A. R. M. Bradbury, J. M. Oliver, W. S. Hlavacek, and B. Wilson. Crosslinking of FceRI with a new trivalent ligand: Structural insights into signal initiation and negative regulation. *under submission*, 2012.

[14] J. J. McGregor. Backtrack search algorithms and the maximal common subgraph problem. *Software: Practice and Experience*, 12(1):23–34, 1982.

[15] M. I. Monine, R. G. Posner, P. B. Savage, J. R. Faeder, and W. S. Hlavacek. Modeling multivalent ligand-receptor interactions with steric constraints on configurations of cell-surface receptor aggregates. *Biophysical Journal*, 98(1):48–56, 2010.

[16] E. F. Pettersen, T. D. Goddard, C. C. Huang, G. S.

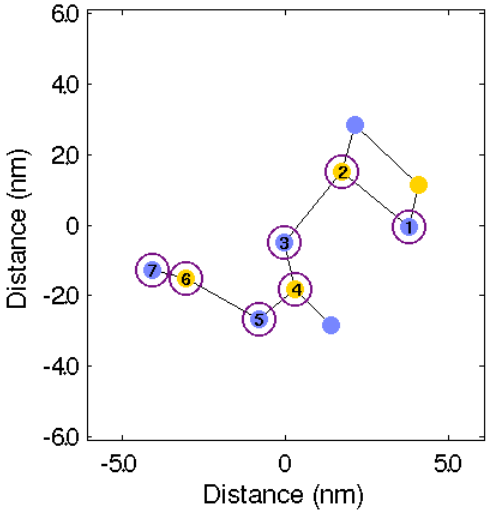

(a) Aggregate 1

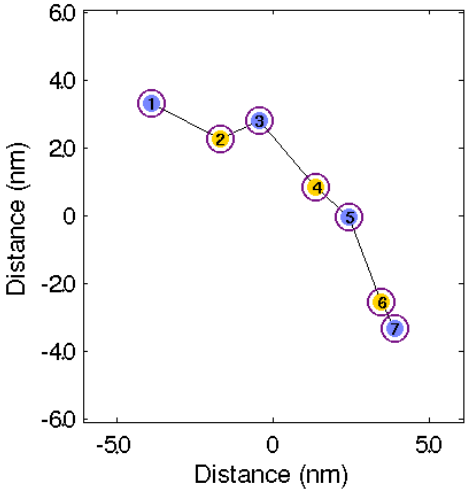

(b) Aggregate 2

Figure 8: Subgraph Isomorphism between 2 aggregates from the 90R/90L ratio run. The first (*top*) is a Complex Aggregate and the second (*bottom*) is a Linear Chain. The purple rings outline the most common subgraph structure and the numbers label the correspondence between the graphs.

Couch, D. M. Greenblatt, E. C. Meng, and T. E. Ferrin. Ucsf chimera–a visualization system for exploratory research and analysis. *Journal of Computational Chemistry*, 25(13):1605–1612, 2004.

[17] J. H. Reif. Complexity of the mover's problem and generalizations. In *Proc. IEEE Symp. Foundations of Computer Science (FOCS)*, pages 421–427, San Juan, Puerto Rico, October 1979.

[18] J. Rivera and A. M. Gilfillan. Molecular regulation of mast cell activation. *Journal of Allergy and Clinical Immunology*, 117(6):1214–1225, 2006.

[19] J. Siek, L.-Q. Lee, and A. Lumsdaine. *The Boost Graph Library: User Guide and Reference Manual*. Addison-Wesley, 2002.

[20] D. Sil, J. B. Lee, D. Luo, D. Holowka, and B. Baird. Trivalent ligands with rigid DNA spacers reveal structural requirements for IgE receptor signaling in RBL mast cells. *ACS Chemical Biology*, 2(10):674–684, 2007.

[21] A. P. Singh, J.-C. Latombe, and D. L. Brutlag. A motion planning approach to flexible ligand binding. In *Int. Conf. on Intelligent Systems for Molecular Biology (ISMB)*, pages 252–261, 1999.

[22] L. Sompayrac. *How the Immune System Works*. J. Wiley & Sons, Sussex, UK, 4th edition, 2012.

[23] X. Tang, S. Thomas, L. Tapia, D. P. Giedroc, and N. M. Amato. Simulating RNA folding kinetics on approximated energy landscapes. *J. Mol. Biol.*, 381:1055–1067, 2008.

[24] L. Tapia, S. Thomas, and N. M. Amato. A motion planning approach to studying molecular motions. *Communications in Information and Systems*, 10(1):53–68, 2010.

[25] S. Thomas, X. Tang, L. Tapia, and N. M. Amato. Simulating protein motions with rigidity analysis. *J. Comput. Biol.*, 14(6):839–855, 2007.

[26] B. S. Wilson, J. M. Oliver, and D. S. Lidke. Spatio-temporal signaling in mast cells. *Advances in Experimental Medicine and Biology*, 716:91–106, 2011.

[27] B. S. Wilson, J. R. Pfeiffer, and J. M. Oliver. Observing FcεRI signaling from the inside of the mast cell membrane. *J. of Cell Biol.*, 149:1131–1142, 2000.

[28] B. S. Wilson, J. R. Pfeiffer, Z. Surviladze, E. A. Gaudet, and J. M. Oliver. High resolution mapping of mast cell membranes reveals primary and secondary domains of FcεRI and LAT. *J. of Cell Biol.*, 14:645–658, 2001.

[29] Y. Wu, J. Vendome, L. Shapiro, A. Ben-Shaul, and B. Honig. Transforming binding affinities from three dimensions to two with application to cadherin clustering. *Nature*, 475:510–513, 2011.

[30] K. Xu, B. Goldstein, D. Holowka, and B. Baird. Kinetics of multivalent antigen DNP-BSA binding to IgE-FcεRI in relationship to the stimulated tyrosine phosphorylation of FcεRI. *J. Immunol.*, 160(7):3225–3235, 1998.

[31] J. Yang, M. I. Monine, J. R. Faeder, and W. S. Hlavacek. Kinetic Monte Carlo method for rule-based modeling of biochemical networks. *Phys. Rev. E*, 78(3):031910, 2008.